Azuma and Katayama *Earth, Planets and Space* (2017) 69:8
DOI 10.1186/s40623-016-0593-z

Earth, Planets and Space

FULL PAPER

Open Access

Evolution of the rheological structure of Mars

Shintaro Azuma[1,2,3*] and Ikuo Katayama[1]

Abstract

The evolution of Mars has been greatly influenced by temporal changes in its rheological structure, which may explain the difference in tectonics between Mars and Earth. Some previous studies have shown the rheological structures of Mars calculated from the flow law of rocks and the predicted thermal structure. However, the Peierls mechanism, which is the dominant deformation mechanism at relatively low temperature, and the evolution of water reservoirs on Mars were not considered in such studies. In this paper, we apply the Peierls mechanism to refine the rheological structure of Mars to show a new history of the planet that considers the most recent reports on its evolution of water reservoirs. Considering the Peierls creep and the evolution of water reservoirs, we attempt to explain why the tectonics of Mars is inactive compared with that of Earth. On early Mars, the lithospheric thickness inferred from the brittle–ductile transition was small, and the lithospheric strength was low (~200–300 MPa) under wet conditions at 4 Gya. This suggests that plate boundaries could have developed on the early "wet" Mars, which is a prerequisite for the operation of plate tectonics. Our results also imply that the lithospheric strength had significantly increased in the Noachian owing to water loss. Therefore, plate tectonics may have ceased or could no longer be initiated on Mars. At the least, the tectonic style of Mars would have dramatically changed during the Noachian.

Keywords: Mars, rheological structure, time evolution, plate tectonics

Background

Mars is a terrestrial planet and, like Earth, is composed of rock and metal. There is no standing liquid water, advanced surface life, or plate tectonics on Mars, suggesting that Mars and Earth followed different evolutionary paths (e.g., Zuber 2001). Plate tectonics is a convection style that dominates the material circulation between a planetary surface and its interior. Therefore, the absence of plate tectonics on Mars could have significantly influenced its evolution. Previous studies have discussed the possibility of plate tectonics on Mars in the past (e.g., Sleep 1994; Connerney et al. 1999; Schubert et al. 2001; Breuer and Spohn 2003). Sleep (1994) proposed that the crustal dichotomy on Mars was produced by past plate tectonics because crustal thinning over an 8000-km-wide region in the northern lowlands of Mars is unlikely without plate tectonics. In contrast, it has been suggested, based on gravity and topography data of Mars, that the crustal dichotomy was formed by a giant impact (Andrews-Hanna et al. 2008). Connerney et al. (1999, 2005) suggested that the magnetic lineation patterns observed by *Mars Global Surveyor* (MGS) provide evidence for plate tectonics or plate divergence on Mars. However, there is no other evidence for plate divergence on Mars. Therefore, the occurrence of plate tectonics on Mars remains a matter of debate. The initiation of plate tectonics requires a lithosphere of moderate thickness and plate boundaries (i.e., a lithosphere of moderate strength; e.g., Solomatov and Moresi 1996; Tackley 1998). To consider the history of planetary tectonics, the lithospheric strength and thickness should be evaluated from the calculated rheological structures.

Rheological structure, which represents the deformation behavior and strength of the planetary interior, plays an important role in the evolution of planets because it controls the existing type of planetary convection (Solomatov and Moresi 1996; Hauck and Phillips 2002;

*Correspondence: azuma.shintaro.937@m.kyushu-u.ac.jp
[3] Department of Earth and Planetary Science, Kyushu University, 744 Motooka, Nishi-Ku, Fukuoka 819-0395, Japan
Full list of author information is available at the end of the article

Korenaga 2009). The rheological behavior of planetary interiors is sensitive to temperature, water, and chemical composition (e.g., Frost and Ashby 1982; Karato and Wu 1993; Karato and Jung 2003), which may produce strong rheological layering and change the lithospheric strength (Burgmann and Dresen 2008). The present-day Martian lithosphere is inferred to be thick, rigid, and immobile compared with that on Earth, resulting in a one-plate planet (Schubert et al. 1990). However, it is expected that the rheological structure has changed throughout Martian history. Some previous studies report the rheological structure of Mars and its evolution (e.g., Grott and Breuer 2008). In such studies, power-law creep, in which the strain rate is proportional to a power of stress, was used to infer the rheological structure in a region of ductile deformation (e.g., Grott and Breuer 2008; Ruiz et al. 2008; Grott and Breuer 2010), although the Peierls mechanism, which is the dominant deformation mechanism at low temperature (<~1000 °C), was not applied. In this mechanism, the strain rate is exponentially proportional to the applied stress (Fig. 1; Tsenn and Carter 1987). Figure 1b shows the deformation mechanism map for wet olivine ($P = 1$ GPa, $d = 1$ mm) in which the deformation mechanism changes with temperature and strain rate. Assuming a power-law creep may lead to overestimation of the lithospheric strength (Fig. 1a). Moreover, recent studies and observations report that the dramatic water loss occurred during the Noachian on Mars (Kurokawa et al. 2014) and that phyllosilicates such as smectite, chlorite, serpentine, and saponite have been found in several Noachian terrain areas (e.g., Bibring et al. 2006; Ehlmann et al. 2009, 2010). This information may change our understanding of the rheological structures and environments of Mars and thus need to be considered when the rheological structure is calculated to evaluate the history of Martian tectonics. Therefore, the main objective of this study is to present the rheological structure of the Martian lowlands (North Pole) and highlands (Solis Planum) and its temporal evolution, as calculated from flow laws and a temperature profile derived from present-day heat-producing element (HPE) abundances (Hahn et al. 2011; Ruiz et al. 2011). The present study differs from previous studies in three main ways. We develop a suitably complex rheological model of the Martian lithosphere using appropriate flow laws for rock, including the Peierls mechanism. In addition, we consider the evolution of water and the existence of phyllosilicates during the evolution of the rheological structure of Mars. Finally, we evaluate the temporal changes in lithospheric strength and tectonics on Mars. The past and present rheological structures offer new insights into the evolution of the Martian interior and its tectonics.

Calculation of temperature profiles

In our model, the Martian interior is separated into four sections: crust, chemically depleted mantle, primordial

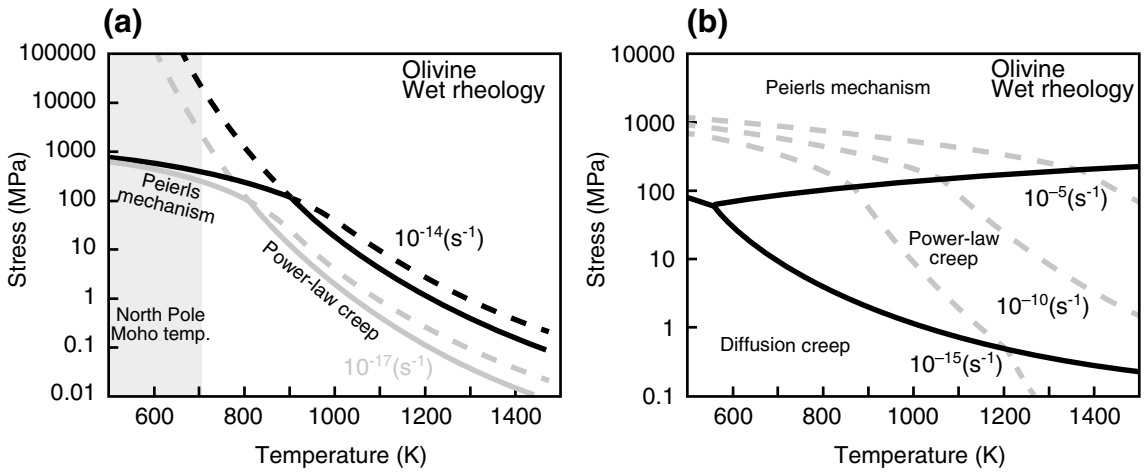

Fig. 1 **a** Creep curves of wet olivine as functions of stress and temperature at strain rates of 10^{-14} (*black lines*) and 10^{-17} (*gray lines*) s^{-1}. These creep curves were calculated from the Peierls mechanism (Katayama and Karato 2008) and power-law creep (Karato and Jung 2003). *Solid lines* indicate the dominant mechanism and stress required to achieve the assumed strain rate at each temperature. At high temperature, power-law creep was the dominant deformation mechanism, although the stress of the power-law creep exceeded that of the Peierls mechanism below ~1000 K. This suggests that the Peierls mechanism becomes dominant at low temperature and high stress. The *shaded section* shows variations in the temperature of the Moho at the North Pole (Fig. 4). **b** Deformation mechanism map for wet olivine. Stress is plotted as a function of temperature at $P = 1.0$ GPa and grain size of 1.0 mm. The *thick solid line* represents the transition of the deformation mechanism, and the *dashed lines* show different strain rates at 10^{-5}, 10^{-10}, and 10^{-15} (s^{-1}). The transitions between the deformation mechanism of olivine were calculated for diffusion creep (grain boundary diffusion; Hirth and Kohlstedt 2003), power-law creep (Karato and Jung 2003), and the Peierls mechanism (Katayama and Karato 2008)

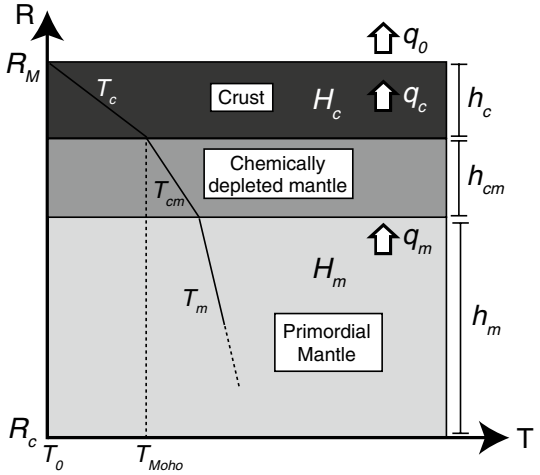

Fig. 2 Conceptual model of Martian thermal structure used in this study for calculations. In our model, the Martian interior is separated into crust, chemically depleted mantle, mantle, and core

Table 1 Parameters for calculation of thermal structure in Mars

	North Pole*	Solis Planum
Crustal density ρc (kg/m^3)	2900[a]	2900[a]
Crustal thickness hc (km)	35[b]	65[c]
Crustal thermal conductivity kc (W/m K)	2.5[d]	2.5[d]
Mantle density ρm (kg/m^3)	3300	3300
K (ppm)	3659[e]	2540[e]
Th (ppm)	0.69[e]	0.42[e]
U (ppm)	0.18[e]	0.11[e]
Surface temperature T_0 (K)	155[b]	220[f]
Martian radius R_M (km)	3390	
Core radius R_c (km)	1700[g]	
Surface gravity g (ms^{-2})	3.71	
Gas constant R (JK^{-1}mol^{-1})	8.3144	

[a] Ruiz (2014), [b] Phillips et al. (2008), [c] Neumann et al. (2004), [d] Kobranova (1989), [e] Hahn et al. (2011), [f] Kieffer et al. (1977), [g] Yoder et al. (2003)

* HPE abundances are average values for Martian crust

Table 2 Rates of heat release *H* and half-lives of the radioactive isotopes

	H (W/kg)	Half-lives τ (yr)	Abundance ratio (%)
^{238}U	9.46×10^{-5}	4.47×10^{9}	99.28
^{235}U	5.69×10^{-4}	7.04×10^{8}	0.71
U	9.81×10^{-5}		
^{232}Th	2.64×10^{-5}	1.40×10^{10}	100
^{40}K	2.92×10^{-5}	1.25×10^{9}	0.0119
K	3.48×10^{-9}		

These parameters are from Turcotte and Schubert (2002)

mantle, and core (Fig. 2). The evolution of the temperature profile for Mars was calculated from surface heat flow and heat production by using the steady heat conduction equation (Turcotte and Schubert 2002). The crustal geotherm T_c, the geotherm of chemically depleted mantle T_{cm}, and the mantle geotherm T_m are, respectively, given by:

$$T_c = T_0 + \frac{q_0}{k_c} y - \frac{\rho_c H_c}{2k_c} y^2, \tag{1}$$

$$T_{cm} = T_{Moho} + \frac{q_m}{k_y}(y - h_c) \tag{2}$$

and

$$T_m = T_{bcm} + \frac{q_m}{k_y}(y - (h_c + h_{cm})) - \frac{\rho_m H_m}{2k_y}(y - (h_c + h_{cm}))^2, \tag{3}$$

where q_0 and q_m are the surface heat flow and mantle heat flow, respectively; ρ_c and ρ_m are the density of the crust and mantle, respectively; y is depth; H_c and H_m are the heat production of the crust and mantle, respectively; T_0 and T_{Moho} are the surface temperature and the estimated Moho temperature, respectively; T_{bcm} is the temperature at the bottom of chemically depleted mantle; h_c is the Moho depth; and k_c and k_y are the thermal conductivities of the crust and mantle, respectively. It should be noted that the chemically depleted mantle is depleted in radiogenic heat-producing elements; heat production is negligible in such mantle (Fig. 2). The parameters used in Eqs. (1) and (2) are summarized in Tables 1 and 2. Xu et al. (2004) reported that changes in the thermal conductivity of olivine, based on changes in temperature and pressure, obey the relationship

$$k = k_{298}\left(\frac{298}{T}\right)^{\lambda}(1 + aP), \tag{4}$$

where k_{298} is the thermal conductivity at room temperature, and λ and a are constants. We used values of $\lambda = 1/2$ and $a = 0.032$ GPa^{-1}, which are adopted from Xu et al. (2004). The thermal conductivity of olivine at a depth of y (km) can be calculated from the relationship

$$k_y = k_{298}\left(\frac{298}{T_{y-1}}\right)^{\lambda}(1 + aP_y). \tag{5}$$

Surface heat flow q_0 can be calculated from crustal heat flow and mantle heat flow. Therefore, the surface heat flow q_0 is given by:

$$q_0 = q_c + q_m = \rho_c + H_c h_c + q_m, \tag{6}$$

where q_c is the crustal heat flow derived from heat-producing elements (Eq. 5). The total present-day heat production H_c in the Martian crust is calculated from the concentration of heat-producing elements as determined from Gamma Ray Spectrometer (GRS) data (Hahn et al. 2011) and from the rates of heat release presented by Turcotte and Schubert (2002). In our calculation, the Martian crust is assumed to be vertically homogeneous in terms of chemical composition and the resultant distribution of incompatible radiogenic isotopes (e.g., Boynton et al. 2007; Hahn et al. 2011). In contrast, the total radiogenic heat from the Martian mantle is assumed to be equal to the average value of the total radiogenic heat in Martian crust (e.g., Hahn et al. 2011). This assumption was derived from the estimation of bulk planetary chemistry and the behavior of the incompatible heat-producing elements during the formation of the crust (Taylor et al. 2006; Wanke and Dreibus 1988; Hahn et al. 2011). Therefore, mantle heat flow in Mars is given by:

$$q_m = \frac{Q_c}{A_m} = \frac{\rho_c V_c H_{ca}}{A_m}, \tag{7}$$

where Q_c and V_c are the total crustal heat and crustal volume, respectively; A_m is the surface area of Martian mantle, and H_{ca} is the crustal heat production derived from the average concentration of heat-producing elements in the crust. In the calculation of the crustal volume V_c, the average crustal thickness is assumed to be 45 km (Neumann et al. 2004). Mantle heat production is given by:

$$H_m = \frac{q_m}{\rho_m h_m}, \tag{8}$$

where h_m is the thickness of primordial mantle (Fig. 2), in which the chemically depleted mantle is assumed to be 100 km thick. To calculate the present-day mass concentrations of individual radioactive elements in the Martian mantle, we first determined the abundance of uranium C_0^U, which can be related to the heat production H_m, calculated using Eq. (8), and the heat generation rates of individual radioactive elements as follows (Turcotte and Schubert 2002):

$$H_m = C_0^U \left(H^U + \frac{C_0^{Th}}{C_0^U} H^{Th} + \frac{C_0^K}{C_0^U} H^K \right). \tag{9}$$

The ratios of K to U and Th to U, which are required to determine the abundance of U (C_0^U) in the Martian mantle, are assumed to be $C_0^K/C_0^U = 10^4$ and $C_0^{Th}/C_0^U = 3.8$ (Turcotte and Schubert 2002; Meyer 2003). Surface heat flow and mantle heat flow in the past were obtained from past total heat production in the crust and mantle. The past total heat production H on Mars can be related to the heat generation rate, half-life ($\tau_{1/2}$), and present-day mass concentration of individual radioactive elements C_0 as follows (Turcotte and Schubert 2002):

$$\begin{aligned} H = {} & 0.9928 C_0^U H^{U238} \exp\left(\frac{t \ln 2}{\tau_{1/2}^{U238}} \right) \\ & + 0.0071 C_0^U H^{U235} \exp\left(\frac{t \ln 2}{\tau_{1/2}^{U235}} \right) \\ & + C_0^{Th} H^{Th} \exp\left(\frac{t \ln 2}{\tau_{1/2}^{Th}} \right) \\ & + 1.19 \times 10^{-4} C_0^K H^{K40} \exp\left(\frac{t \ln 2}{\tau_{1/2}^{K40}} \right). \end{aligned} \tag{10}$$

The heat generation rate and half-life $\tau_{1/2}$ of each radioactive isotope are summarized in Table 2; the abundances of heat-producing elements in the Martian crust have been reported previously (Hahn et al. 2011).

Figure 3 shows the surface heat flow and mantle heat flow of the Martian North Pole and Solis Planum thorough time, as calculated above. Although Solis Planum is depleted in heat-producing elements relative to other regions (Table 1), its heat flow tends to be higher than that at the North Pole because the crustal thickness is thicker at the former than that at latter (Fig. 3).

Calculation of rheological structure

The rheological structures of the lowlands (North Pole) and highlands (Solis Planum) were inferred by using the temperature profiles of each region, as calculated above. The rheological structure in regions of brittle deformation was determined from the frictional strengths of dry and wet rock. Frictional strength is sensitive to normal stress as follows:

$$\tau = \mu \sigma_n + C_f, \tag{11}$$

where τ is the shear stress at which frictional sliding begins, μ is the friction coefficient, σ_n is the normal stress, and C_f is the frictional cohesive strength. Byerlee (1978) revised Eq. (11) more explicitly. According to Byerlee's law, the friction coefficient μ is 0.85 for $3 < \sigma_n < 200$ MPa, whereas $\mu = 0.6$ for $\sigma_n > 200$ MPa. However, the frictional strength of plate boundaries on Earth is weak. For example, the San Andreas Fault (SAF) has a frictional coefficient of $\mu = 0.15$ owing to the presence of the clay mineral saponite (Lockner et al. 2011). Morrow et al. (2000) used friction experiments to show that the frictional coefficient of phyllosilicates dramatically decreases under conditions of water saturation. Phyllosilicates formed by aqueous alteration have been found in several areas of Noachian terrain on Mars (Bibring et al. 2006; Ehlmann et al. 2009, 2010). Therefore, we used not only Byerlee's law but also the

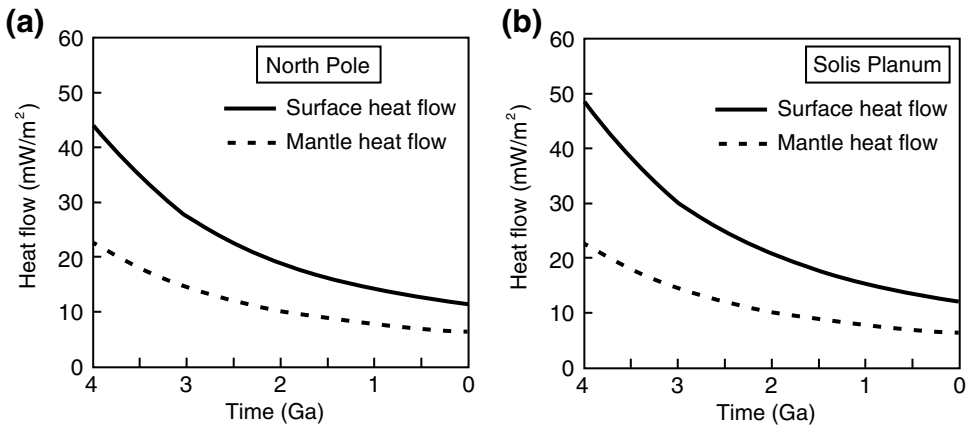

Fig. 3 Heat flow at the North Pole and Solis Planum on Mars. **a** Surface heat flow (*solid line*) and mantle heat flow (*dashed line*) as a function of time at the North Pole. The surface heat flow was calculated from the crustal and mantle heat flows (Eq. 5). The mantle heat flow was calculated by assuming that the total radiogenic heat from the Martian mantle is equal to the average value of the total radiogenic heat in the Martian crust (Eq. 6). **b** Surface heat flow (*solid line*) and mantle heat flow (*dashed line*) as functions of time at Solis Planum

frictional coefficient of the SAF as the frictional strength of the phyllosilicates.

Shear stress in Eq. (11) should be converted to differential stress and compared with that given by flow laws for regions of plastic deformation (e.g., Kohlstedt et al. 1995). Shear stress τ and normal stress σ_n can be converted to differential stress by considering the force balance in the fault system as follows:

$$\sigma_n = \sigma_1 \sin^2\theta + \sigma_3 \cos^2\theta \tag{12}$$

$$\tau = (\sigma_1 - \sigma_3)\sin\theta\cos\theta, \tag{13}$$

where θ is the angle between the fault strike and the direction of maximum principal stress. In converting shear stress to differential stress, we assume a fault in which the angle θ is 30° (Kohlstedt et al. 1995). In regions of brittle deformation, the assumption of liquid water on the surface enables us to consider a wet Mars because such water affects the pore pressure P_p (e.g., Terzaghi and Peck 1967). The pore pressure P_p influences the effective stress σ_{eff} of each principal stress as follows:

$$\sigma_{\text{eff}} = \sigma_n - \alpha_p P_p, \tag{14}$$

where the coefficient α_p is assumed to be 1. The pore pressure P_p is generally obtained from the lithostatic pressure P_l and the parameter λ as follows:

$$\lambda = \frac{P_p}{P_l}. \tag{15}$$

We assumed the hydrostatic pore pressure, for which $\lambda = 0.38$. Based on the above calculation, the rheological structure in the region of brittle deformation is inferred in terms of frictional strength.

In regions of ductile deformation, rock strength at any given depth is calculated from viscous flow laws that represent the strength of solids, which are dependent on strain rate, temperature, and chemical composition (Frost and Ashby 1982; Karato and Jung 2003). Rock strength at any depth is given by:

$$\dot{\varepsilon} = A\frac{\sigma^n}{d^m}\exp\left(-\frac{H^*}{RT}\right), \tag{16}$$

where $\dot{\varepsilon}$ is the strain rate, A is a constant, σ is the stress, n is the stress exponent, d is grain size, m is the grain size exponent, H^* is the activation enthalpy, and T is temperature (Poirier 1985). In power-law creep, the stress exponent and grain size exponent are generally 3 and 0, respectively. In diffusion creep, the stress exponent and grain size exponent are 1 and 3, respectively. Because diffusion creep (grain boundary diffusion) is the dominant deformation mechanism in high-temperature regions (Fig. 1b) equivalent to deeper Martian conditions, it does not influence the rheological structure in the present study. Although power-law creep and diffusion creep occur at high temperatures, the Peierls mechanism is dominant at low temperatures and high stress rates (Tsenn and Carter 1987; Katayama and Karato 2008; Demouchy et al. 2013). In the Peierls mechanism, the strain rate is exponentially proportional to the applied stress, as follows:

$$\dot{\varepsilon} = A\sigma^2\exp\left(-\frac{H^*}{RT}\left(1-\left(\frac{\sigma}{\sigma_p}\right)^p\right)^q\right), \tag{17}$$

where σ_p is the Peierls stress, and p and q are non-dimensional parameters that depend on the geometry of kinks

(Kocks et al. 1975). Strain rates of 10^{-16} and 10^{-19} are assumed at Solis Planum (McGovern et al. 2004; Ruiz et al. 2006). In contrast, because deformation at the North Pole is likely caused by loading due to the north polar layered deposits (NPLD; Phillips et al. 2008), it follows that deformation at the North Pole depends on the timescale of climate change due to Martian obliquity cycles (Laskar et al. 2002, 2004). Laskar et al. (2002) reported that polar caps may preserve climatic records spanning the last few million years. Based on this report, if the loading age of NPLD is assumed to be ~5 m.y. (Phillips et al. 2008), a strain rate of 10^{-14} (s^{-1}) appears to be plausible (Laskar et al. 2004). However, the strain might not reach the elastic limit (Sleep 2015), and it is possible that the lithosphere at the North Pole deforms elastically because of the NPLD. In addition to the strain rate of 10^{-14} (s^{-1}), we calculated the yield strength envelope for a strain rate of 10^{-16} (s^{-1}), which is a typical value for terrestrial intraplate regions (e.g., Tesauro et al. 2007). Other parameters used in Eqs. (16) and (17) are summarized in Table 3.

In regions of ductile deformation, intracrystalline water should be assumed to consider a wet Mars. The presence of intracrystalline water has a strong influence on rock rheology (e.g., Hirth and Kohlstedt 2003; Karato and Jung 2003), and rock strength is significantly reduced by increased water content. The effect of water on creep rate is usually calculated by:

$$\dot{\varepsilon} \propto C_{\mathrm{OH}}^{\gamma}. \tag{18}$$

where C_{OH} is the water content and γ is the water content exponent (e.g., Hirth and Kohlstedt 2003; Karato and Jung 2003). Thus, the flow law for a water-rich environment in a closed system with respect to water is described by:

$$\dot{\varepsilon} = A\frac{\sigma^n}{d^m}C_{\mathrm{OH}}^{\gamma}\exp\left(-\frac{H^*}{RT}\right). \tag{19}$$

In this study, a wet rheology indicates a rock that is water-saturated at Moho conditions, with water contents of ~10,000 ppm H/Si in plagioclase and ~1000 ppm H/Si in olivine. This indicates that the rheological structures presented in this study represent the lower (wet rheology) and upper (dry rheology) limits of brittle–ductile transition (BDT) depth and lithospheric strength.

Results

The temperature profiles of the Martian lowlands (Northern Plains) and highlands (Solis Planum) were calculated every 1 billion years by using the present-day crustal abundances of radioactive isotopes ^{235}U, ^{235}U, ^{232}Th, and ^{40}K and their half-lives (Fig. 4). In our thermal model, we assumed that the surface heat flow is derived from crustal heat flow and mantle heat flow (Eq. 5). The temperature gradient of crust beneath the North Pole is low compared with that at the Solis Planum because the North Pole has a low crustal heat production owing to thin crustal thickness. In relatively deep portions of the mantle, the thermal gradient becomes steep owing to reduced thermal conductivity (Eq. 4; Fig. 4). Although Solis Planum is depleted in radioactive isotopes (Hahn et al. 2011), the thick crustal depth in this region results in relatively large crustal heat production. As a result, the temperature gradient in this region is relatively high despite a low concentration of radiogenic heat-producing elements. It should be noted, however, that our thermal model does not include the heat released upon cooling of the mantle; therefore, our temperature profiles have lower limits. For example, Baratoux et al. (2011) reported the relatively high potential mantle temperature of Mars during the

Table 3 Parameters of flow law

Rock type	Creep mechanism	A (s^{-1} MPa^{-n} μm^{m})	*n*	*m*	*r*	σ_p (MPa)	*E* (kJ/mol)	*V* (cm^3/mol)	Reference
Plagioclase (wet)	Diffusion creep	$10^{1.7}$	1	3	–	–	170	–	Rybacki and Dresen (2000)
	Dislocation creep	$10^{-5.6}$	3.9	–	–	–	235		Shelton (1981)
	Peierls creep	$10^{-1.23}$	2	–	–	3410	235	–	Azuma et al. (2014)
Plagioclase (dry)	Diffusion creep	$10^{12.1}$	1	3	–	–	467	–	Rybacki and Dresen (2000)
	Dislocation creep	$10^{0.9}$	4	–	–	–	431	–	Shelton (1981)
	Peierls creep	$10^{3.48}$	2	–	–	9831	431	–	Azuma et al. (2014)
Olivine (wet)	Diffusion creep	$10^{6.0}$	1	3	1	–	335	4	Hirth and Kohlstedt (2003)
	Dislocation creep	90	3.5	–	1.2	–	480	11	Hirth and Kohlstedt (2003)
	Peierls creep	$10^{0.67}$	2	–	1.2	2870	410	11	Katayama and Karato (2008)
Olivine (dry)	Diffusion creep	$10^{9.2}$	1	3	–	–	375	5	Hirth and Kohlstedt (2003)
	Dislocation creep	1.1×10^5	3.5	–	–	–	530	14	Hirth and Kohlstedt (2003)
	Peierls creep	$10^{6.7}$	2	–	–	9600	510	14	Katayama and Karato (2008)

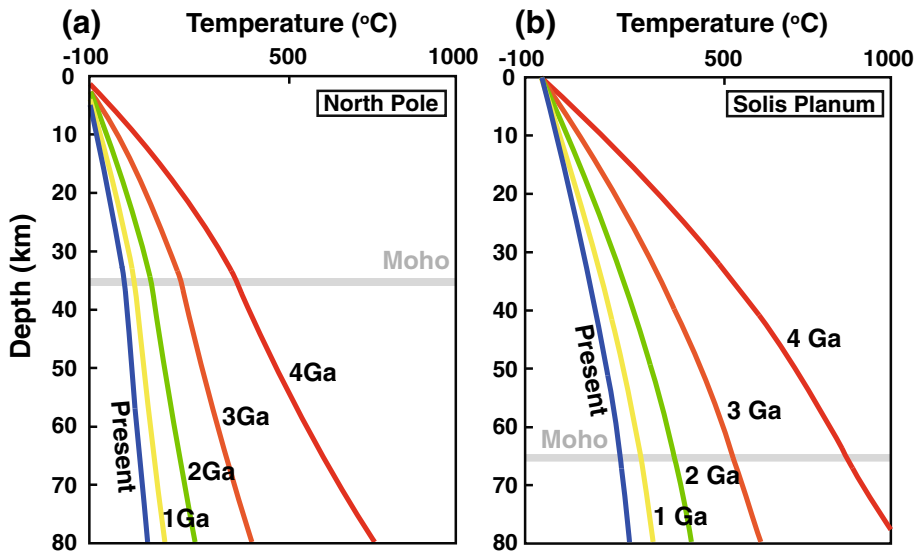

Fig. 4 Temperature profiles every 1 billion years on Mars calculated from the surface heat flow and the present-day abundance of radioactive isotopes. **a** Temperature profile of the Martian North Pole. The surface temperature and the Moho depth were assumed to be 155 K and 35 km (Phillips et al. 2008), respectively. **b** Temperature profiles of the Martian highlands (Solis Planum). The surface temperature and the Moho depth were assumed to be 220 K (Kieffer et al. 1977) and 65 km (Neumann et al. 2004), respectively

Hesperian–Amazonian based on the chemical composition and the degree of partial melting in volcanic provinces. Conversely, Phillips et al. (2008) reported that the elastic thickness at the present-day North Pole is significantly large (>300 km), indicating that the temperature of the Mars interior should be low at the present-day North Pole. Further observations and analyses are needed to constrain the thermal model of the Martian interior.

On the basis of the calculated temperature profiles (Fig. 4), we determined the rheological structure of Mars for every 1 billion years by using plagioclase and olivine flow laws (Figs. 5, 6, 7). Figure 5 shows the calculated rheological structures of Mars including the present-day North Pole and Solis Planum. To quantitatively evaluate the rheological structure, the strength at the BDT should be compared between each rheological structure. The BDT is a transition in deformation behavior from brittle failure to viscous flow. The stress required to induce brittle failure increases with depth because it depends on pressure, whereas the strength in viscous flow decreases with depth owing to temperature dependence. Therefore, the lithospheric strength at the BDT, where frictional strength and viscous strength are crossed in rheological structures, is the maximum strength of the lithosphere. In this paper, lithospheric strength is defined as the strength at the BDT. The strength of the lithosphere for a wet rheology is weaker than that for a dry rheology. The BDT in the present-day North Pole lowlands is deeper (>100 km) and stronger (>3000 MPa for dry rheology) than that in the oceanic lithosphere on Earth (~35–40 km, ~800 MPa; Kohlstedt et al. 1995), suggesting that the thickness of the present-day Martian lithosphere is greater than that of Earth. Given that the frictional strength in the region of brittle deformation is proportional to the normal stress (Eq. 11), the rock strength in the brittle region of Earth tends to be higher than that on Mars owing to differences in gravity. On the contrary, rock strength in the ductile region is sensitive to temperature; therefore, a cooler Mars has a rigid and thick lithosphere. For the Martian Solis Planum highlands, the BDT depth has been inferred from observed thrust faults to be >25 km (Golombek et al. 2001; Ruiz et al. 2006). The results of our study on the rheological structure of the highlands show that the BDT depth is ~30 km for a wet rheology and >~80 km for a dry rheology. The depth of thrust faults reported in previous studies can be reproduced only under wet conditions.

Figures 6 and 7 show the evolution of the rheological structure of the Martian North Pole and Solis Planum, respectively. In both cases, the rheological structure for a dry rheology shows marked temporal changes in strength. In contrast, the rheological structure for a wet rheology shows relatively gradual temporal changes in strength and in structure. A comparison between present and past Mars shows that the BDT of present-day Mars is deeper than that of past Mars, suggesting that the lithospheric thickness of present-day Mars is greater than that of past Mars (Figs. 5, 6, 7). The rheological structure

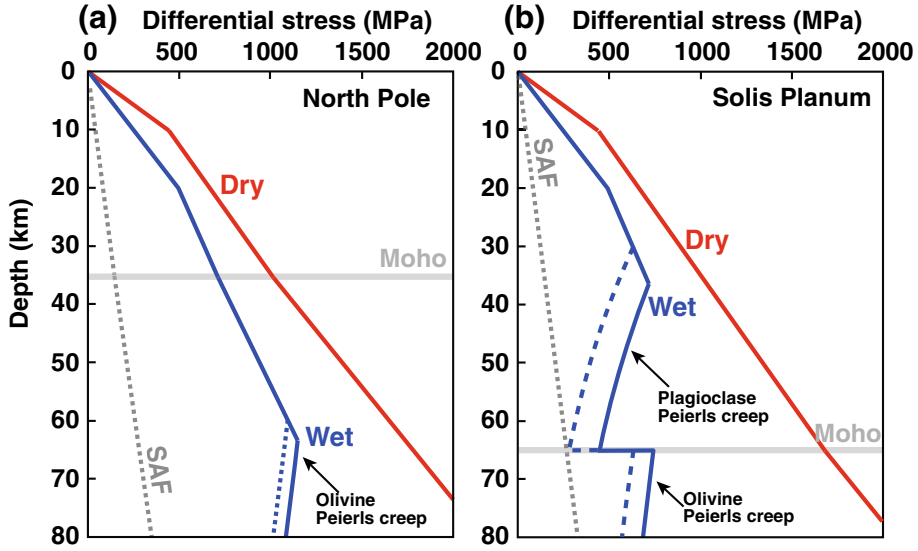

Fig. 5 Strength profile models of present-day Mars. Strength in the brittle deformation region was calculated by using Byerlee's law (Byerlee 1978). The *dashed line* labeled SAF shows the frictional strength of the San Andreas Fault, for which $\mu = 0.15$ (Lockner et al. 2011). The Peierls mechanism, power-law creep, and diffusion creep (grain boundary diffusion) were applied to calculate the strength of minerals at each depth in the region of ductile deformation. The flow law of plagioclase (Shelton 1981; Rybacki and Dresen 2000; Azuma et al. 2014) was used for the crust, and the flow law of olivine (Evans and Goetze 1979; Karato and Wu 1993; Karato and Jung 2003; Hirth and Kohlstedt 2003; Katayama and Karato 2008) was applied for the mantle. The strain rates were assumed to be 10^{-14} s^{-1} (*solid line*) and 10^{-16} s^{-1} (*dashed line*) for the North Pole (Laskar et al. 2004), and strain rates of 10^{-16} (*solid line*) and 10^{-19} s^{-1} (*dashed line*) were adopted for Solis Planum (McGovern et al. 2004; Ruiz et al. 2006). The parameters used are summarized in Table 3; the rheological structure for both dry and wet rheologies is shown. **a** Strength profile models for the Martian lowlands (North Pole). The Moho depth was assumed to be 35 km (Phillips et al. 2008). **b** Strength profile models of the Martian highlands (Solis Planum). The Moho depth was assumed to be 65 km (Neumann et al. 2004)

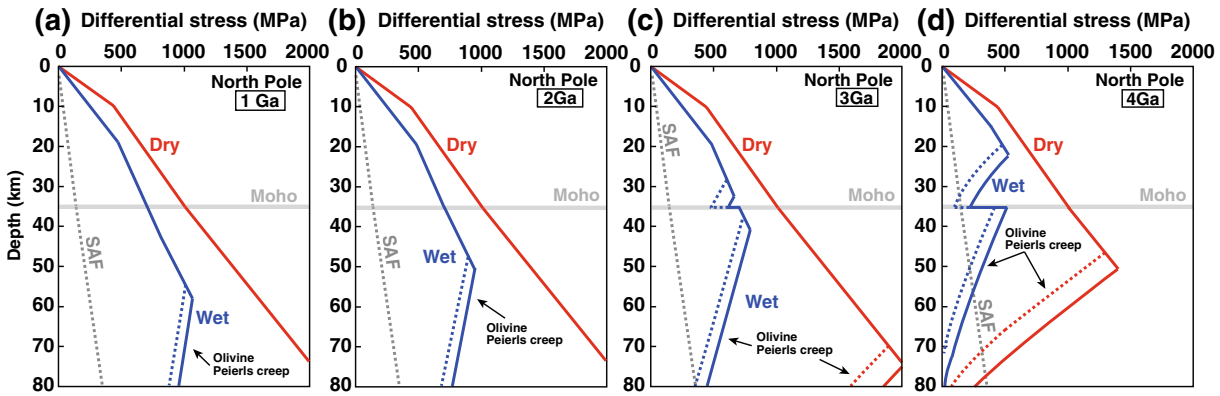

Fig. 6 Strength profile for the past North Pole every 1 billion years. The rheological structure of the past North Pole was predicted from the temperature profile (Fig. 4a). Strength in the brittle deformation region was calculated by using Byerlee's law (Byerlee 1978). In the region of ductile deformation, the Peierls mechanism, power-law creep, and diffusion creep (grain boundary diffusion) were applied to calculate the strength at each depth, as shown in Fig. 5. The strain rate was assumed to be 10^{-14} (*solid line*) or 10^{-16} s^{-1} (*dashed line*). The parameters used are summarized in Table 3; the rheological structure for both dry (*red lines*) and wet (*blue lines*) rheologies is shown. The *dashed line* labeled SAF shows the frictional strength of the San Andreas Fault, for which $\mu = 0.15$ (Lockner et al. 2011)

of past Mars (Figs. 6, 7) indicates that the strength and depth of the BDT were similar to those of the present-day Earth, as proposed by Kohlstedt et al. (1995). For example, the BDT at the North Pole under wet conditions was 1–2 Ga and that at Solis Planum under dry and wet conditions was 4 Ga. This result suggests that the

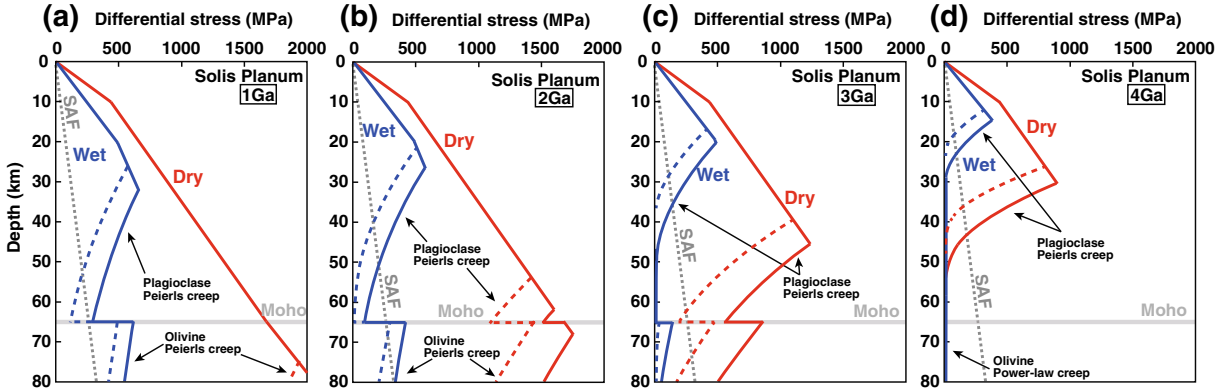

Fig. 7 Strength profiles of the past Martian highlands (Solis Planum). Based on the temperature profile (Fig. 4b), the rheological structure of the Martian highlands every 1 billion years is calculated as per Fig. 5. The strain rate is assumed to be 10^{-16} (*solid line*) or 10^{-19} s^{-1} (*dashed line*)

past Martian interior might have been similar to that of present-day Earth, even if past Mars was under strictly dry conditions.

Discussion

Rheological structures at the North Pole and Solis Planum

Rheological structures should be modeled by appropriate depth-dependent deformation mechanisms. Most previous studies consider only power-law creep (Eqs. 16, 19) as a deformation mechanism for planetary crust and mantle in calculations of lithospheric strength and thickness and in numerical simulations of mantle convection (e.g., Solomatov and Moresi 1997; Mackwell et al. 1998; Grott and Breuer 2008). However, recent experimental studies of rock rheology have reported that the Peierls mechanism plays an important role in rock deformation at relatively low temperature and high stress (Katayama and Karato 2008; Demouchy et al. 2013). Our calculations show that the Peierls mechanism is dominant at relatively shallow depths under our assumptions (Figs. 5, 6, 7), indicating that the application of power-law creep to a low-temperature region ($T < 1000$ °C) leads to an overestimation of lithospheric strength and thickness.

The rheological structure indicates the existence of an incompetent layer and a strength contrast between the crust and mantle; therefore, knowledge of the rheological structure is key to understanding the evolution of planetary interiors. Incompetent layers are usually defined as those having yield strengths of less than 10–20 MPa or a yield strength that does not exceed 1–5% in lithostatic pressure (Burov and Diament 1995). The existence of incompetent crust has a strong influence on the elastic thickness (McNutt et al. 1988; Grott and Breuer 2010), and the strength contrast across the Moho in terrestrial planets may result in mechanical decoupling between the crust and mantle (Burov and Diament 1995; Azuma et al. 2014). For example, a weak lower crust (incompetent layer) that cannot support the tectonic stress (e.g., bending stress) may allow a strong upper crust (competent layer) to deform independently of the mantle lithosphere (Burov and Diament 1995).

Under dry conditions, the calculated rheological structure shows no strength contrast across the Moho at the present-day Martian North Pole, indicating that the crust and mantle are mechanically coupled (Fig. 5a). This means that a convecting mantle may influence planetary surface motion, as is the case for Earth's oceanic lithosphere. This also suggests that surface load of the NPLD directly affects the mantle deformation. Similarly, under water-saturated conditions, the rheological structure of the North Pole has no strength contrast between the crust and mantle, which prevented decoupling from occurring at the Moho even under wet conditions (Fig. 6a).

In the present-day Solis Planum, the strength contrast across the Moho under dry conditions is nonexistent, suggesting that the crust and mantle are mechanically coupled (Fig. 5). Under wet conditions, however, the lithosphere in the Solis Planum has a strength contrast between the crust and mantle, which may have caused the mechanical decoupling at this boundary.

The rheological structures for the past North Pole and Solis Planum show variations in terms of strength contrast, incompetent crust, strength, and BDT depth (Figs. 5, 6, 7). In the North Pole region, under dry conditions, there is no incompetent crustal layer and no strength contrast throughout Martian history (Fig. 6). In contrast, under wet conditions, a strength contrast exists from 4 to 3 Ga, indicating that decoupling may have occurred between the crust and mantle in the past North Pole. Throughout Martian history, no incompetent crustal layer formed under wet conditions, indicating that the

effect of the incompetent crustal layer, which reduces the elastic thickness beneath the North Pole, is nonexistent.

In contrast to the North Pole, the lithosphere beneath the past Solis Planum experienced a strength contrast for a relatively long time, which suggests mechanical decoupling between the crust and mantle from 2 Ga to the present day under wet conditions (Figs. 5, 7). The incompetent crust that existed from 3 to 2 Ga under wet conditions likely contributed to the small elastic thickness (24–37 km) in the Solis Planum (e.g., McGovern et al. 2002, 2004; Ruiz et al. 2006). The observed thin elastic thickness at Solis Planum in the Hesperian era might be attributed to the existence of incompetent crust produced under wet conditions.

Evolution of the BDT and lithospheric strength

On present-day Mars, it is believed that stagnant-lid convection is dominant and that convection occurs only beneath the thick, rigid, and immobile lithosphere (e.g., Solomatov and Moresi 1997). Although plate tectonics does not appear to have occurred on present-day Mars, previous studies have discussed whether plate-like tectonics have occurred on Mars in the past (e.g., Sleep 1994; Connerney et al. 1999; Schubert et al. 2001; Breuer and Spohn 2003). Importantly, the initiation of plate tectonics requires moderate lithospheric thickness and faulting on a sufficient scale to form plate boundaries (e.g., Nimmo and McKenzie 1998; Tackley 1998, 2000); therefore, the lithosphere must have moderate strength ($\leq$200–300 MPa) for plate tectonics to occur. In this section, we discuss the time evolution of the lithospheric thickness and strength on Mars.

Figure 8 shows the BDT depth for the North Pole and Solis Planum as a function of time under both dry and wet conditions. Although the BDT depth is not identical to the lithospheric thickness, the two are closely linked, and the convection style and lithosphere thickness are coupled. On present-day Mars, the BDT depth for a dry rheology is significantly deeper than that for a wet rheology in both the North Pole and Solis Planum regions. This occurred because the existence of water reduces the frictional strength in regions of brittle deformation owing to pore pressure and also reduces rock strength in regions of ductile deformation. A comparison of the present-day North Pole and Solis Planum revealed that the BDT depth at the North Pole is markedly deeper under both wet and dry conditions, indicating that lithospheric thickness in the North Pole region is greater than that of the Solis Planum. This is likely attributed to differences in the present-day thermal structure and in crustal thickness (e.g., Zuber et al. 2000). The BDT depth in Solis Planum tends to be relatively shallow owing to the thicker crust (Figs. 7, 8b).

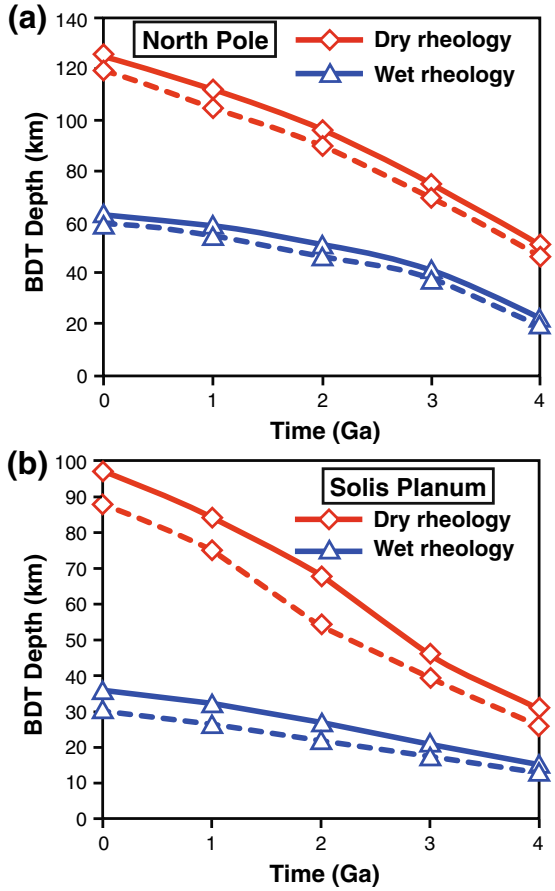

Fig. 8 Depth of brittle–ductile transition (BDT) as a function of time. The BDT of the Martian lowlands (North Pole) and highlands (Solis Planum) under dry and wet conditions was obtained from the calculated strength profile models (Figs. 5, 6, 7). **a** BDT depth of the North Pole as a function of time under dry and wet conditions. The strain rates of 10^{-14} (*solid line*) and 10^{-16} s^{-1} (*dashed line*) are from Laskar et al. (2004), Phillips et al. (2008), and Tesauro et al. (2007). The BDT depth has increased with time. Under wet conditions, the depth of the BDT has shown a moderate increase. In contrast, the BDT depth has increased more rapidly under dry conditions compared with wet rheology. **b** Changes in BDT depth in the Martian highlands (Solis Planum) for strain rates of 10^{-16} s^{-1} (*solid line*) and 10^{-19} s^{-1} (*dashed line*) under dry (*red lines*) and wet (*blue lines*) conditions

Water also plays an important role in the temporal changes in BDT depth. In models of the Martian past, at both the North Pole and Solis Planum, the BDT for a wet rheology is shallower than that for a dry rheology; this suggests a thin lithosphere in water-rich environments (Fig. 8). For both wet and dry rheologies, the BDT depth in both regions tends to increase with time, suggesting that the net thickness of the lithosphere could have changed throughout Martian history. The BDT depth would have increased more rapidly under dry conditions than that in a wet rheology (Fig. 8). According to these

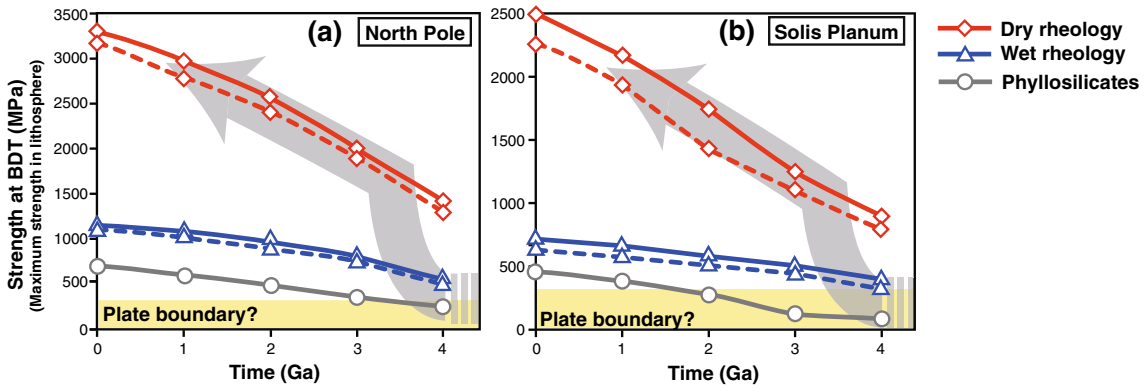

Fig. 9 Maximum lithospheric strength at the North Pole and Solis Planum on Mars as a function of time. The maximum lithospheric strength was calculated from the rheological structures determined in this study. Shaded sections represent the range of lithospheric strength that allows the planetary surface to form plate boundaries (e.g., Tackley 2000). Heavy *arrows* indicate the evolution of lithospheric strength on Mars, as inferred from water loss during the Noachian. **a** Evolution of the lithospheric strength at the North Pole under dry (*red lines*) and wet (*blue lines*) conditions. The *gray line* indicates the lithospheric strength that considers the frictional coefficient of hydrous phyllosilicates. The strain rates of 10^{-14} (*solid lines*) and 10^{-16} (*dashed lines*) s^{-1} are from Laskar et al. (2004), Phillips et al. (2008), and Tesauro et al. (2007). **b** Evolution of the lithospheric strength at Solis Planum for strain rates of 10^{-16} s^{-1} (*solid lines*) and 10^{-19} s^{-1} (*dashed lines*) under dry (*red lines*) and wet (*blue lines*) conditions. The *gray line* indicates the result that consider the frictional coefficient of hydrous phyllosilicates

calculations, the lithospheric structure and its evolution could be quite different depending on whether the past conditions on Mars were dry or wet. The thick lithosphere under dry conditions may have resulted in stagnant-lid convection, whereas a relatively thin lithosphere under wet conditions would have been a necessary condition for the development of narrow plate boundaries.

Figure 9 shows the temporal evolution of the maximum lithospheric strength in the Martian lowlands and highlands based on the calculated rheological structures (Figs. 5, 6, 7). The upper limit of lithospheric strength that enables the planetary surface to form a plate boundary is also shown in Fig. 9 (e.g., Tackley 2000). Under dry conditions, the lithospheric strength of Mars (red lines) would have increased from 4 Ga to the present day. Under dry conditions, the lithospheric strengths are significantly higher than the required threshold values (~200–300 MPa). In contrast, the lithospheric strength for a wet rheology (blue and gray lines) would have undergone relatively gradual temporal changes. The lithospheric strength considering the frictional coefficient of phyllosilicates (gray lines) is presumably the lower limit of lithospheric strength under wet conditions. At 4 Ga, the values of wet lithospheric strength can satisfy the threshold values, which may have enabled the development of plate boundaries. The observed geological data indicate that the wet environment of Mars was limited to the Noachian era, as described above (e.g., Bibring et al. 2006; Ehlmann et al. 2009, 2010). Although the wetness of the surface is not directly connected to the wetness of the deep interior, the near-surface strength of the lithosphere is influenced because water loss at the Martian surface would have increased the frictional strength of phyllosilicates and decreased the pore pressure in fault zones. On the basis of hydrogen isotope data (D/H) of Martian meteorites and theoretical calculations, Kurokawa et al. (2014) suggested that the water loss was greatest during the pre-Noachian. This result may indicate the possibility that the deep interior of Mars experienced dehydration. Therefore, the lithospheric strength might have changed from wet to dry conditions after the pre-Noachian, as indicated by the heavy arrows in Fig. 9.

These analyses of lithospheric thickness (Fig. 8) and strength (Fig. 9) suggest that water plays a key role in the evolution of planetary interiors. The initiation of plate tectonics on past Mars is likely to have required water, and the lithospheric strength may have changed dramatically owing to water loss during the Noachian (Fig. 9). These results suggest the possibility that Martian tectonics also changed with the rheological structure after the pre-Noachian. Although it is difficult to determine whether plate tectonics occurred on Mars based on analyses of rheological structure alone, it is important to perform convection simulations based on the rheological structures proposed in this study.

Conclusion

We presented the rheological structure of Mars and its time evolution, and we discussed the evolution of the Martian interior. The rheological structure of Mars determined in this study indicates that shallow deformation on Mars was controlled mostly by the Peierls mechanism and that the application of power-law creep alone leads to an overestimation of lithospheric strength. The

rheological structures on Mars should therefore be calculated by using the Peierls mechanism in addition to power-law creep. Our results show that the lithosphere of past Mars had moderate strength owing to the presence of water during the Noachian. In addition, the rheological structures and lithospheric strength of Mars may have changed owing to water loss later in Martian history. Therefore, Mars lost its capability to develop plate boundaries, which are necessary for the initiation of plate tectonics.

We provided a more realistic rheological structure of the Martian lithosphere in this study. The next step toward understanding Martian planetary evolution is to evaluate the rheological structure beneath large Martian mountains such as Olympus. Gravity and topography data for large Martian mountains have been used to estimate the strength of the Martian lithosphere in previous studies (e.g., Arkani-Hamed 2000); however, these studies consider only power-law creep and use linear thermal gradients. To adequately account for the complex evolution of the Martian lithosphere, future work should re-evaluate the rheological structure beneath large Martian mountains and should test whether the calculated lithosphere could sustain large mountains such as Olympus.

In our models, the thermal structures were based on the abundance of radiogenic heat-producing elements in the crust for each region (Hahn et al. 2011). More accurate thermal structures would require direct observation of surface heat flow. A new NASA lander, *Interior Exploration Using Seismic Investigations, Geodesy and Heat Transport* (InSight), will be launched in 2018. This mission to Mars will place a seismometer and heat-flow probe on the surface to provide more accurate, detailed information on the interior of the planet. We look forward to new opportunities for exciting research into the mysteries of Martian planetary evolution.

Authors' contributions

SA calculated the thermal structure and the evolution of rheological structure on Mars. SA and IK contributed to the discussion and implications. IK helped to improve the manuscript. SA and IK read and approved the final manuscript. Both authors read and approved the final manuscript.

Author details

[1] Department of Earth and Planetary Systems Science, Hiroshima University, Kagamiyama 1-3-1, Higashi-Hiroshima 739-8526, Japan. [2] Earth-Life Science Institute, Tokyo Institute of Technology, 2-12-1, Ookayama, Meguro-Ku, Tokyo 152-8550, Japan. [3] Department of Earth and Planetary Science, Kyushu University, 744 Motooka, Nishi-Ku, Fukuoka 819-0395, Japan.

Acknowledgements

The authors thank T. Nakakuki and K. Okazaki for offering advice and encouragement. Data supporting Fig. 4 is provided in Tables 1, 2. Data supporting Figs. 5, 6, 7 are provided in Table 3. This study was supported by the Global Career Design Center at Hiroshima University, Japan.

Competing interests

The authors declare that they have no competing interests.

Received: 18 June 2016 Accepted: 20 December 2016
Published online: 03 January 2017

References

Andrews-Hanna JC, Zuber MT, Benerdt WB (2008) The Borealis basin and the origin of the martian crustal dichotomy. Nature 453(7199):1212–1215. doi:10.1038/nature07011

Arkani-Hamed J (2000) Strength of Martian lithosphere beneath large volcanoes. J Geophys Res 105:26713–26732

Azuma S, Katayama I, Nakakuki T (2014) Rheological decoupling at the Moho and implication to Venusian tectonics. Sci Rep 4:4403. doi:10.1038/srep04403

Baratoux D, Toplis MJ, Monnereau M, Gasnault O (2011) Thermal history of Mars inferred from orbital geochemistry of volcanic provinces. Nature 472:338–341. doi:10.1038/nature09903

Bibring J-P, Langevin Y, Mustard JF, Poulet F, Arvidson R, Gendrin A, Gondet B, Mangold N, Pinet P, Forget F, the OMEGA team (2006) Global mineralogical and aqueous mars history derived from OMEGA/Mars express data. Science 312:400–404

Boynton WV, Taylor GJ, Evans LG, Reedy RC, Starr R, Janes DM, Kerry KE, Drake DM, Kim KJ, Williams RMS, Crombie MK, Dohm JM, Baker V, Metzger AE, Karunatillake S, Keller JM, Newsom HE, Arnold JR, Brückner J, Englert PAJ, Gasnault O, Sprague AL, Mitrofanov I, Squyres SW, Trombka JI, d'Uston L, Wanke H, Hamara DK (2007) Concentration of H, Si, Cl, K, Fe, and Th in the low and mid latitude regions of Mars. J Geophys Res 112: E12S99. doi:10.1029/2007JE002887

Breuer D, Spohn T (2003) Early plate tectonics versus single-plate tectonics on Mars: evidence from magnetic field history and crust evolution. J Geophys Res 108(E7):5072. doi:10.1029/2002JE001999

Burgmann R, Dresen G (2008) Rheology of the lower crust and upper mantle: evidence from rock mechanics, geodesy, and field observations. Ann Rev Earth Planet Sci 36:531–567

Burov EB, Diament M (1995) The effective elastic thickness (T_e) of continental lithosphere: what does it really mean? J Geophys Res 100:3905–3927

Byerlee JD (1978) Friction of rocks. Pure appl Geophys 116:615–626

Connerney JEP, Acuna MH, Wasilewski P, Ness NF, Reme H, Mazelle C, Vignes D, Lin RP, Mitchell D, Cloutier P (1999) Magnetic lineations in the ancient crust of Mars. Science 284:794–798

Connerney JEP, Acuna MH, Ness NF, Kletetschka G, Mitchell DL, Lin RP, Reme H (2005) Tectonic implications of Mars crustal magnetism. Proc Natl Acad Sci USA 102(42):14970–14975

Demouchy S, Tommasi A, Ballaran TB, Cordier P (2013) Low strength of Earth's uppermost mantle inferred from tri-axial deformation experiments on dry olivine crystals. Phys Earth Planet Inter 220:37–49

Ehlmann BL, Mustard JF, Swayze GA, Clark RN, Bishop JL, Poulet F, Des Marais DJ, Roach LH, Milliken RE, Wray JJ, Barnouin-Jha O, Murchie SL (2009) Identification of hydrated silicate minerals on Mars using MRO-CRISM: geologic context near Nili Fossae and implications for aqueous alteration. J Geophys Res 114:E00D08. doi:10.1029/2009JE003339

Ehlmann BL, Mustard JF, Murchie SL (2010) Geologic setting of serpentine deposits on Mars. Geophys Res Lett 37:L06201. doi:10.1029/2010GL042596

Evans B, Goetze C (1979) The temperature variation of hardness of olivine and its implication for polycrystalline yield stress. J Geophys Res 84:5505–5524

Frost HJ, Ashby MF (1982) Deformation-mechanism Maps: the plasticity and creep of metals and ceramics. Pergamon Press, Oxford

Golombek MP, Anderson FS, Zuber MT (2001) Martian wrinkle ridge topography: evidence for subsurface faults from MOLA. J Geophys Res 106:23811–23821

Grott M, Breuer D (2008) The evolution of the Martian elastic lithosphere and implications for crustal and Mantle rheology. Icarus 193:503–515. doi:10.1016/j.icarus.2007.08.015

Grott M, Breuer D (2010) On the spatial variability of the Martian elastic lithosphere thickness: evidence for mantle plumes? J Geophys Res 115:E03005. doi:10.1029/2009JE003456

Hahn BC, McLennan SM, Klein EC (2011) Martian surface heat production and crustal heat flow from Mars Odyssey Gamma-Ray spectrometry. Geophys Res Lett 38:L14203. doi:10.1029/2011GL047435

Hauck SA, Phillips RJ (2002) Thermal and crustal evolution of Mars. J Geophys Res 107(E7):5052. doi:10.1029/2001JE001801
Hirth G, Kohlstedt DL (2003) Rheology of the upper mantle and the mantle wedge: A view from the experimentalists. In: Eiler J (ed) Inside the subduction factory. Geophy. Monog. Ser., vol 138. AGU, Washington, pp 83–105
Karato S, Jung H (2003) Effects of pressure on high-temperature dislocation creep in olivine. Phil Mag A83:401–414
Karato S, Wu P (1993) Rheology of the upper mantle: a synthesis. Science 260:771–778. doi:10.1126/science.260.5109.771
Katayama I, Karato S (2008) Low-temperature, high-stress deformation of olivine under water-saturated conditions. Phys Earth Planet Inter 168:125–133
Kieffer HH, Martin TZ, Peterfreund AR, Jakosky BM, Miner ED, Palluconi FD (1977) Thermal and albedo mapping of Mars during the Viking primary mission. J Geophys Res 82:4249–4291
Kobranova VN (1989) Petrophysics. Springer, Berlin
Kocks UF, Argon AS, Ashby MF (1975) Thermodynamics and kinetics of slip. Prog Mater Sci 19:1–291
Kohlstedt DL, Evans B, Mackwell SJ (1995) Strength of lithosphere: constraints imposed by laboratory experiments. J Geophys Res 100:17587–17602
Korenaga J (2009) Scaling of stagnant-lid convection with Arrhenius rheology and the effects of mantle melting. Geophys J Int 179:154–170
Kurokawa H, Sato M, Ushioda M, Matsuyamab T, Moriwaki R, Dohmd JM, Usui T (2014) Evolution of water reservoirs on Mars: constraints from hydrogen isotopes in Martian meteorites. Earth Planet Sci Lett 394:179–185
Laskar J, Levrard B, Mustard JF (2002) Orbital forcing of the Martian polar layered deposits. Nature 419:375–377
Laskar J, Correia ACM, Gastineau M, Joutel F, Levrard B, Robutel P (2004) Long-term evolution and chaotic diffusion of the insolation quantities on Mars. Icarus 170:343–364
Lockner DA, Morrow C, Moore D, Hickman S (2011) Low strength of deep San Andreas fault gouge from SAFOD core. Nature 472:82–85
Mackwell SJ, Zimmerman ME, Kohlstedt DL (1998) High-temperature deformation of dry diabase with application to tectonics on Venus. J Geophys Res 103(B1):975–984
McGovern PJ, Solomon SC, Smith DE, Zuber MT, Simons M, Wieczorek MA, Phillips RJ, Neumann GA, Aharonson O, Head JW (2002) Localized gravity/topography admittance and correlation spectra on Mars: implications for regional and global evolution. J Geophys Res 107(E12):5136. doi:10.1029/2002JE001854
McGovern PJ, Solomon SC, Smith DE, Zuber MT, Simons M, Wieczorek MA, Phillips RJ, Neumann GA, Aharonson O, Head JW (2004) Correction to "Localized gravity/topography admittance and correlation spectra on Mars: implications for regional and global evolution". J Geophys Res 109:E07007. doi:10.1029/2004JE002286
McNutt MK, Diament M, Kogan MG (1988) Variations of elastic plate thickness at continental thrust belts. J Geophys Res 93:8825–8838
Meyer C (2003) Mars meteorite compendium. Lyndon B. Johnson Space Center, NASA, Houston
Morrow CA, Moore DE, Lockner DA (2000) The effect of mineral bond strength and adsorbed water on fault gouge frictional strength. Geophys Res Lett 27:815–818
Neumann GA, Zuber MT, Wieczorek MA, McGovern PJ, Lemoine FG, Smith DE (2004) Crustal structure of Mars from gravity and topography. J Geophys Res 109:E08002. doi:10.1029/2004JE002262
Nimmo F, McKenzie D (1998) Volcanism and tectonics on Venus. Ann Rev Earth Planet Sci 26:23–51
Phillips RJ, Zuber MT, Smrekar SE, Mellon MT, Head JW, Tanaka KL, Putzig NE, Milkovich SM, Campbell BA, Plaut JJ, Safaeinili A, Seu R, Biccari D, Carter LM, Picardi G, Orosei R, Mohit PS, Heggy E, Zurek RW, Egan AF, Giacomoni E, Russo F, Cutigni M, Pettinelli E, Holt JW, Leuschen CJ, Marinangeli L (2008) Mars north polar deposits: stratigraphy, age, and geodynamical response. Science 320:1182–1185
Poirier JP (1985) Creep of crystals. Cambridge University Press, New York
Ruiz J (2014) The early heat loss evolution of Mars and their implications for internal and environmental history. Sci Rep 4:4338. doi:10.1038/srep04338
Ruiz J, Tejero R, McGovern PJ (2006) Evidence for a differentiated crust in Solis Planum, Mars, from lithospheric strength and heat flow. Icarus 180:308–313
Ruiz J, Fernandez C, Gomez-Ortiz D, Dohm JM, Lopez V, Tejero R (2008) Ancient heat flow, crustal thickness, and lithospheric mantle rheology in the Amenthes region. Mars Earth Planet Sci Let 270(1–2):1–12
Ruiz J, McGovern PJ, Jiménez-Díaz A, López V, Williams J-P, Hahn BC, Tejero R (2011) The thermal evolution of Mars as constrained by paleo-heat flows. Icarus 215:508–517
Rybacki E, Dresen G (2000) Dislocation and diffusion creep of synthetic anorthite aggregates. J Geophys Res 105:26017–26036
Schubert G, Bercovici D, Glatsmaier GA (1990) Mantle dynamics in Mars and Venus: influence of an immobile lithosphere on three dimensional mantle convection. J Geophys Res 95(B9):14105–14129
Schubert G, Turcotte DL, Olson P (2001) Mantle convection in the Earth and Planets. Cambridge University Press, New York
Shelton GL (1981) Experimental deformation of single phase and polyphase crustal rocks at high pressures and temperatures, Ph. D. thesis, Brown University, Providence
Sleep NH (1994) Martian plate tectonics. J Geophys Res 99(E3):5639–5655
Sleep NH (2015) Long-term deformation driven by small ambient tectonic stresses and strong oscillating tidal within Enceladus with analogy to rock behavior near the San Andreas Fault. Geochem Geophys Geosyst 16:1670–1686. doi:10.1002/2015GC005725
Solomatov VS, Moresi L-N (1996) Stagnant lid convection on Venus. J Geophys Res 101(E2):4737–4753
Solomatov VS, Moresi L-N (1997) Three regimes of mantle convection with non-Newtonian viscosity and stagnant lid convection on the terrestrial planets. J Geophys Res 24(15):1907–1910
Tackley PJ (1998) Self-consistent generation of tectonic plates in three-dimensional mantle convection. Earth Planet Sci Lett 157:9–22
Tackley PJ (2000) Self-consistent generation of tectonic plates in time-dependent, three-dimensional mantle convection simulations 1. Pseudoplastic yielding, Geochem Geophys Geosyst 1:1021. doi:10.1029/2000GC000036
Taylor GJ, Stopar JD, Boynton WV, Karunatillake S, Keller JM, Brückner J, Wänke H, Dreibus G, Kerry KE, Reedy RC, Evans LG, Starr RD, Martel LMV, Squyres SW, Gasnault O, Maurice S, d'Uston C, Englert P, Dohm JM, Baker VR, Hamara D, Janes D, Sprague AL, Kim KJ, Drake DM, McLennan SM, Hahn BC(2006) Variations in K/Th on Mars. J Geophys Res 111:E03S06. doi:10.1029/2006JE002676
Terzaghi K, Peck RB (1967) Soil mechanics in engineering practice. Wiley, New York, p 729
Tesauro M, Kaban MK, Cloeting SAPL, Hardebol NJ, Beekman F (2007) 3D strength and gravity anomalies of the European lithosphere. Earth Planet Sci Lett 263:56–73
Tsenn MC, Carter NL (1987) Upper limits of power law creep of rocks. Tectonophysics 136:1–26
Turcotte DL, Schubert G (2002) Geodynamics, 2nd edn. Cambridge University Press, New York, pp 132–144
Wanke H, Dreibus G (1988) Chemical composition and accretion history of the terrestrial planets. Philos Trans R Soc Lond Ser A 325:545–557. doi:10.1098/rsta.1988.0067
Xu Y, Shankland TJ, Linhardt S, Rubie DC, Langenhorst F, Klasinski K (2004) Thermal diffusivity and conductivity of olivine, wadsleyite and ringwoodite to 20 GPa and 1373 K. Phys Earth Planet Inter 143–144:321–336
Yoder CF, Konopliv AS, Yuan DN, Standish EM, Folkner WM (2003) Fluid core size of Mars from detection of the solar tide. Science 300:299. doi:10.1126/science.1079645
Zuber MT (2001) The crust and mantle of Mars. Nature 412:220–227. doi:10.1038/35084163
Zuber MT, Solomon SC, Phillips RJ, Smith DE, Tyler GL, Aharonson O, Balmino G, Banerdt WB, Head JW, Johnson CL, Lemoine FG, McGovern PJ, Neumann GA, Rowlands DD, Zhong S (2000) Internal structure and early thermal evolution of Mars from Mars Global Surveyor. Science 287:1788–1793